Title: Photoelectrochemical reduction of CO_2 with TiNT

Authors: M.A.L.R.M. Cortes*[a], S. McMichael[a], J.W.J. Hamilton[a], P.K. Sharma[a], A. Brown[a], J.A. Byrne[a]

[a]NIBEC, Ulster University, Newtownabbey, BT37 0QB, UK

*Corresponding author: ma.cortes@ulster.ac.uk

Abstract

In order to reduce CO_2 emissions and utilise CO_2 as a useful by-product, artificial photosynthesis is being explored for carbon capture and utilisation. Semiconductor photocatalysts excited by solar energy may be used to convert CO_2 to fuels or useful chemicals, e.g. CO, CH_4, CH_3OH. The photocatalytic reduction of CO_2 to useful products has been widely studied in order to overcome the greenhouse effect and the current energy necessities. However, this reaction has proved to be extremely low efficiency when compared to other processes. In order to improve these yields, photoelectrochemical reduction of CO_2 has been considered, since it combines photocatalysis and electrocatalysis. To this end, a two compartment photoelectrochemical cell (PEC) has been designed and fabricated for the reduction of CO_2. This custom built reactor consists of dual phases, where gas phase CO_2 is feed into the cathode comparement and an aqueous phase in the anode compartment. The anode and cathodes for a sandwich were the anode perforated foil on exposing aligned titania nanotubes to electrolyte bonded to nafion; which forms a bridge to Pt deposited carbon cloth cathode electrode in gas phase compartment. CO_2 reduction products were detected with GC connected to the reactor. The PEC reactor improved the yield and the formal quantum efficiency compared to our previous studies using photocatalytic reactors.

Keywords: CO_2 reduction, PEC, photocatalysis, photoelectrocatalysis

1. Introduction

CO_2 is the main greenhouse gas present in the atmosphere and thus one of the main contributors to climate change. To reduce the effect of global warming and match the growing energy demand it is crucial that researchers find renewable energy resources [1]. To that end, artificial

photosynthesis has been considered as one of the methods to convert CO_2 to fuels. The photocatalytic reduction of CO_2 has been widely studied. However, the yields observed are still too low to meet the energy demand [2-5]. Photoelectrochemical reduction of CO_2 is an alternative approach to photocatalytic reduction of CO_2 to convert CO_2 into fuels since it incorporates photocatalysis and electrocatalysis. The main advantages of using a photoelectrochemical cell (PEC) for the reduction of CO_2 is that the sites for oxidation and reduction reactions are spatially separated and recombination reactions can be reduced with an electrochemical bias [6]. In PECs, the two electrodes used are usually submersed in an electrolyte and one or both the electrodes is photoactive. The semiconductor is typically coated on an electrically conducting support to form a semiconductor electrode (either photoanode or photocathode). The anode and cathode may be separated by a proton-conducting membrane to form a sandwich or face each other and share the same electrolyte. Monolithic electrodes with anodes and cathode on opposite sides of the same structure should be porous to allow diffusion of reactants and products, and for ionic conduction within the cell. The reactor can be made from a UV-vis transparent materials or it may be fitted with a transparent window to allow irradiation of the photoelectrodes [5-12]. Reactor geometry is an important factor to take into account when designing a PEC for the reduction of CO_2. The most common PEC geometries are cylindrical, parallel and annular. These conformations will allow a good spatial relation between the light source and the reactor. The choice of material for the window is equally important, with quartz being the most commonly used for its excellent UV transmission [9, 13].

PECs can be divided into three groups, depending on how the semiconductor is used: (1) as a photocathode (p-type), (2) as a photoanode (n-type), or (3) both photocathode and photoanode. With single semiconductor photoelectrodes, the counter electrode is normally metallic. When combining both types of semiconductor, the reactor configuration is photoanode/photocathode, or Z-scheme, when the band gaps and band edges are suitably aligned [5-12, 14]. The reaction in PEC's is usually carried out in gas or liquid phase, and can be performed in batch, semi-batch or continuous flow [6, 12]. Although widely studied, liquid phase PECs present several disadvantages. CO_2 has a low solubility in aqueous solutions which may limit reactant availability leading to lower conversion efficiency. To overcome this drawback, higher pressures that increase the CO_2 concentration in the liquid chamber or alternative electrolytes are needed. Furthermore, aqueous or liquid phase systems cannot run at high temperatures. In a mixed phase PEC, a gas diffusion electrode may be utilised in the cathodic compartment

where CO_2 entering in the gas phase is reduced at the surface of the electrode. This avoids the limited solubility of CO_2, and will also influence the type of product formed [9] Due to the change in availability of other reactants. Mixed phase PECs are designed with two compartments a gas phase section, separated by a proton exchange membrane, into a second compartment with a liquid, typically in the aqueous phase [6, 12].

The first studies ever reported about photoelectrochemical reduction of CO_2 were performed by Halmann in 1978, with a p-type gallium phosphide as a photocathode [15]. Since then, authors have continued investigating the use of PEC for CO_2 reduction [9, 16-20]. At Ulster, Eggins et al. also studied the fixation of CO_2 with visible light active ZnS and CdS photocatalysts [21] and first identified oxalate as a CO_2 reduction product in aqueous phase. More recent studies using PECs for the photoelectrochemical reduction of CO_2, Won et al. used a ZnTe as a photocathode, a saturated calomel electrode (SCE) as reference electrode, and carbon rod as cathode in liquid phase (0.1 M $KHCO_3$ electrolyte) to achieve a faradaic efficiency (FE) of 15.6 % for HCOOH, 5.5 % for CO, and 27.6 % for H_2 was obtained [22]. Whilst Barton et al's reactor was tuned to produce methanol when using an aqueous phase photoelectrochemical cell [17].

Aiming to present the novelty of using a PEC operating in gas phase for the photoelectrocatalytic reduction of CO_2, and compare it to the photocatalytic reduction of CO_2 published previously, a two chamber reactor was designed. A perforated titania nanotube (TiNT) photoanode was used to reduce the proton mass transport, and Pt deposition on carbon cloth (Pt-CC) as the cathode, joined with a Nafion membrane by hot pressing, thereby forming a free standing photoelectrocatalytic disk. Before assembling the disk, both electrode materials were characterised using a Scanning Electron Microscopy (SEM) and Energy Dispersive X-Ray Spectroscopy (EDS). The yields of products obtained were presented in terms of formal quantum efficiency (FQE) to be compared with previous results obtained with the photocatalytic reduction of CO_2 [3] and in faradaic efficiency (FE) to be compared with the literature.

2. Materials and methods

2.1. Electrode preparation for photoelectrochemical studies

Ti foil samples (10 x 20 mm) were cleaned by sonication in Decon 90 detergent (5%) followed by multiple washings and sonication in water. The foils were then washed with ethanol and dried under an Ar stream. TiO_2 (commercial Evonik Aeroxide P25) and hydrothermally prepared nanotubes (denoted NT) with the method described in [3] were immobilised on Ti foil samples (10 x 20 mm) by spray coating until the desired weight was obtained (1 mg). Samples were then annealed at 450°C (Lenton furnace) in air for 2 h (ramp up 2°C min^{-1} and ramp down 2°C min^{-1}).

The aligned titanium nanotubes (TiNT) where produced via anodization using Ti foil as the anode following a method reported previously [23] to obtain the aligned nanotubes. The anodized Ti sheet was rinsed multiple times in distilled water followed by annealing at 450°C in air for 1 h (ramp up 2°C min^{-1} up and ramp down 1°C min^{-1}).

The electrical contacts for all the samples tested (P25, hydrothermally prepared NT, and anodized TiNT) were made by attaching a Cu wire to an area of the foil which had been cleaned previously using abrasive paper following a method reported previously [24]. The contact and any area not coated with TiO_2 was insulated with SU8 photoresist (MicroChem) leaving an active area of 10 x 10 mm^2. The SU8 coated samples were exposed to UV irradiation following the method reported in [24].

2.2. Monolithic Electrode Preparation for PEC Reactor

Ti sheet (50 x 50 mm) was perforated (185 x 1 mm holes). The Ti sheets were then cleaned and anodized following the methods used for the TiNT electrodes as above to produce an anode. The cathode was prepared by electrodepositon of Pt onto porous carbon cloth (Pt-CC) following a method reported previously [25]. Two different potential vs. time regimes were applied: T1 = -0.5 V from 0 to 5s, followed by 0 V until T2. T2 varied from 10 to 600 s until an optimum loading of Pt was obtained. The Pt-CC was then washed with distilled water and dried under an OFN stream (oxygen free nitrogen stream). The anode and cathode were bounded together using nafion sheet as an adhesive layer between the titanium and carbon electrodes. The bonding of the three components was performed by hot pressing for 2 minutes at 120°C and 10 bar min^{-1} (Eurotherm nanodac).

2.4. Materials characterisation

SEM analysis of the anodized TiNT and of the Pt-CC was performed using a Hitachi FESEM SU5000 operated in the potential range of 10 kV at 5 mm working distance. The images were recorded using the secondary electron detector. EDS analysis on the SEM, using the Aztec software, was also performed for the Pt-CC sample.

2.5. Photoelectrochemical studies

The photoelectrochemical studies were conducted on the three described photoelectrodes, in order to access which material would be more suitable for the PEC. In each study the photoelectrode was used as the working electrode in a one compartment cell with a quartz window for irradiation. The counter electrode was a Pt mesh and the reference electrode, a saturated calomel electrode. The supporting electrolyte was 0.1 M $KClO_4$ and a potentiostat (AutoLab) provided electrochemical control. A 450 W Xe lamp, connected to a monochromator (Uniblitz, VMM-T1), was used as the irradiation source (figure S1). The potential, and current, were measured using the General Purpose Electrochemical Software (GPes). Linear sweep voltammetry (LSV) measurements were performed as reported in [24]. The irradiation source was chopped on and off every 10 s for 600 s. Photocurrent was obtained by calculating the difference between the light and dark current. To determine the onset potential for anodic current, the current was measured at fixed potentials in the -1.0 to +1.0 V range, at 0.1 V increments. The potential of the working electrode was kept constant. Once the current reached a steady state (approx. 200 s), the light was then chopped on and off five times every 20 s. Spectral measurements of the samples were performed at a fixed potential of +1.0 V with monochromatic irradiation. The wavelength of the irradiation was applied from 200 to 500 nm, 10nm FWHM, with an increasing wavelength (by 10 nm) recoreded every 20 s of the scan. All potentials are reported against SCE.

The Incident photon-to-current conversion efficiency (IPCE) was calculated [14], using the action spectra of the samples, according to the equation below.

$$IPCE = \frac{number\ of\ electron\ passed\ per\ second}{number\ of\ incident\ photons\ per\ second}\ (eq.\ 1)$$

$$or,\ IPCE\ (\%) = \frac{hc}{e}\left(\frac{j_{photo}(\lambda)}{\lambda P(\lambda)}\right) \times 100\ (eq.\ 2)$$

Where, h is Plank's constant, c is the speed of light, e is the charge of an electron, $J_{photo}\ (\lambda)$ is current density at wavelength λ, and $P(\lambda)$ is the power intensity of the monochromatic illumination [14].

2.6. Photoelectrocatalytic Reactor

The PEC reactor was designed to be assembled from ultra-high vacuum (UHV) stainless steel parts (Swagelok and Kurt J. Lesker) adapted from a version of the photocatalytic reactor used in a previous work [3]. The PEC consisted of a two-electrode configuration with two compartments (liquid and gas phase) separated by a single disk, consisting of an anode and cathode separated by nafion, with an irradiated area of 9.6 cm^2 (figure S2).

The disk was composed of an anodized TiNT photoanode and Pt-CC cathode, separated by a Nafion membrane, preparation discussed previously. $KHCO_3$ (0.5M) was used as the anolyte. A mixture of CO_2:Ar (20:80) was used in the cathode compartment in experimental tests for CO_2 reduction. The reactor was purged for 10 min with the feed gas mixture before sealing at a pressure of 0.5 bar. The reactor was then irradiated with a Xe lamp (100 W, LOT Oriel) through a water IR filter (irradiance spectra can be seen in [3]) with an applied bias of -2 V. The distance between the reactor and the lamp, and the lamp configuration was the same as the one used in [3] to be able to compare the efficiency of the photocatalytic and the photoelectrocatalytic reduction of CO_2.

The gaseous products obtained following irradiation were analysed by gas chromatography (GC) with a flame ionisation detector (FID) and using Helium (BOC, UN1046, 99.999% purity) as a carrier gas. The GC (Agilent Technologies, 7890B) was connected directly to the reactor outlet and samples were analysed after 30 min. The reactor was purged and filled with a range of gas mixtures to provide conditions for CO_2 reduction, or absence of CO_2 for control runs to confirm CO_2 the source of products observed by GC.

2.7 Efficiency

Formal quantum efficiency (FQE) was calculated for the photoelectrocatalytic reduction of CO_2 with the PEC reactor according to the method described in [3]. The distance from the light to the catalyst was kept the same to ensure comparable results. The FQE was calculated using equation 3.

$$FQE = \frac{moles\ of\ electrons\ passed\ to\ form\ products}{moles\ of\ photons\ (\ 250 - 410\ nm, Einsteins)} \quad (eq.\ 3)$$

The photocurrent in the PEC was measured during the duration of the experiment, and the faradaic efficiency was calculated using equation 4 as reported in [26].

$$FE = \frac{Electrons\ transfered\ to\ product}{Total\ electrons\ transfered} = \frac{mnF}{It} \ (eq.\ 4)$$

Where F is Faraday's constant, m is the number of moles of product formed or reactant consumed, n is the number of electrons transferred, I is the short-circuit photocurrent and t is time.

3. Results and Discussion

3.1. Electrode materials characterisation

3.1.1. Pt-CC characterisation
SEM analysis of the different times for the Pt deposition on CC was performed. Samples were denoted according to the deposition time, T_2, i.e. Pt-CC 600s, Pt-CC 300s, Pt-CC 60s, Pt-CC 30s, and Pt-CC 10s.

Figure 1 shows images of the Pt deposition on CC at different T_2. All images were taken with the same magnification and scale (20 k magnification, at 10 kV and 2µm scale) in order to facilitate comparison. In figure 1, the Pt particle size increased with electrodeposition time. It can also be seen that at lower deposition times the platinum particles (figure 1 D) and E)) are more evenly distributed on the carbon cloth, with less particle agglomeration when compared to longer deposition times (figure 1 A), B) and C)). To confirm the presence and the distribution of Pt on CC, EDS was performed.
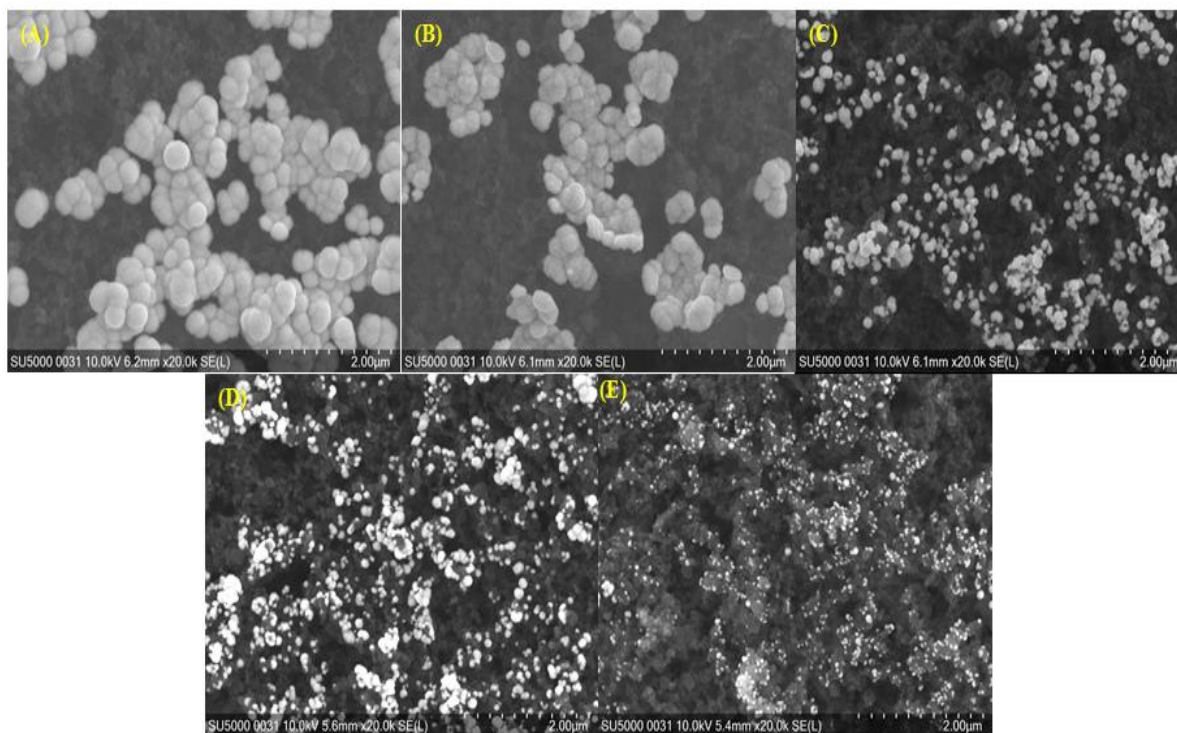
Figure 1 - SEM images of the effect of the deposition time, t_2, on the Pt-CC. (A) Pt-CC 600s, (B) Pt-CC 300s, (C) Pt-CC 60s, (D) Pt-CC 30s, and (E) Pt-CC 10s. All images were taken with a 20 k magnification, at 10 kV and 2μm scale.

For a specific region of Pt-CC (figure 2), EDS signals from the brighter contrast particles in the images, confirm the presence of Pt in the high contrast regions. The peaks obtained for Pt in the spectra (figure S3), correspond to the X- ray energy table, i.e Lα 9.441 keV and Mα 2.050 keV, The presence of F in the spectra is due to the composition of the CC, which contains 3 to 30 % of polytetrafluoroethylene to add hydrophobicity. Using multiple images the average particle size for the lowest T_2, Pt-CC 10s was calculated.
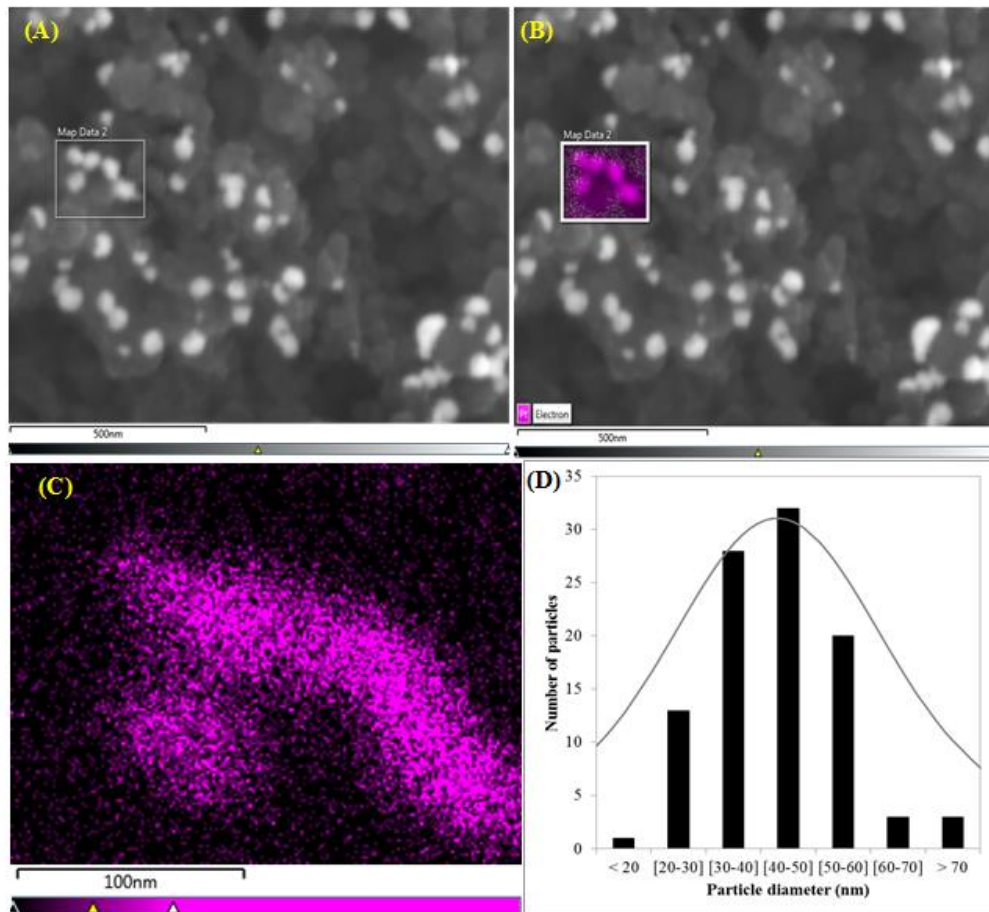
Figure 2 – SEM images and EDS analysis of the Pt-CC with t2=10s. (A) Area selected for the scan, (B) layered image from the analysis of the Pt deposition (Pt detected in pink colour), (C) elemental mapping of the Pt deposition (pink colour), (D) Particle diameter distribution of Pt on CC at T_2=10s

The particle size distribution of Pt on the substrate at T_2=10 s, used as an electrode can be seen in figure 2 (D). The particle size distribution for the other T_2 was not measured. It was observed that the average particle diameter was between 40-50 nm. Particle diameters between 20 and 60 nm were more commonly found when using this electrodeposition time. Duarte et al. [25], only studied the particle diameter for their lowest T_2, which was 60s. The SEM image obtained by Duarte et al. for T_2=60s is in agreement with the one obtained in this work (figure 1 (C)). They obtained their highest number of particles within the range of 70 to 150 nm in diameter, which is two times higher than the one showed in figure 2 (D). This would be expected since the deposition time is higher in Duarte et al work, than the one used in this work.

3.1.2. TiNT characterisation

After anodization and annealing at 450 °C for 1 h, TiNT were analysed with SEM and their average diameter was calculated (figure 3).
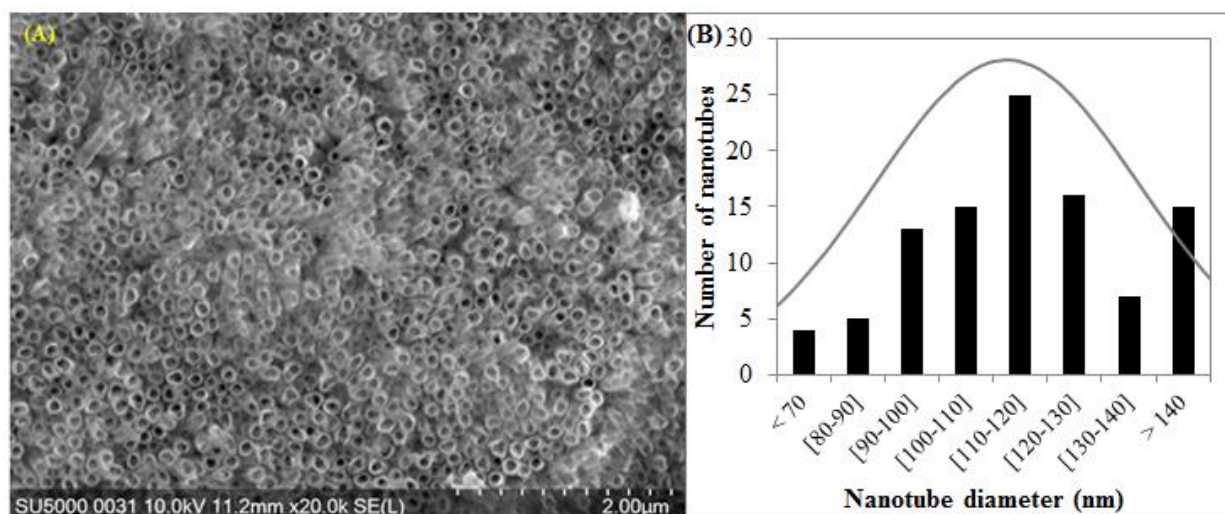

Figure 3 - TiNT characterisation. (A) SEM image of the TiNT (20 k magnification, at 10 kV and 2μm scale), (B) Nanotube diameter distribution

A SEM image of the aligned TiNT can be seen in figure 3 (A). SEM analysis showed that the entire area is uniformly covered with TiNT. The distribution of nanotube diameter obtained through electrochemical anodisation was calculated (figure 3 (B)). It was observed that the majority of the TiNT presented an inner diameter of 110 to 120 nm with a standard deviation of $\pm$ 21 nm. According to the literature, TiNT prepared by electrochemical anodisation usually have an inner diameter on the order of 100 nm [27]. This correlates reasonably with the inner diameter obtained in this study. However, the length and wall thickness of the TiNT were not measured in this work.

3.2. Photoelectrochemical studies

Photoelectrochemical studies were performed on the three photocatalysts. P25 as reference material, hydrothermally prepared NT utilised for photocatalytic CO_2 reduction in a previous work [3] and anodized TiNT. Anodized nanotubes (TiNT) were studied in terms of photoelectrochemical properties as it has previously been reported that TiNTs have a much better photocurrent response than P25 particulate electrodes and their direct formation on Ti foil allows for simple incorporation into a PEC as a photoanode.

The spectral response, measured at a fixed potential of +1.0 V for all three photocatalysts, NT, P25, and TiNT can be seen in figure S4 (A). All samples show photocurrent up to 420 nm, with P25 and TiNT having its highest photocurrent at 350 nm and NT at 320 nm. The spectral response of TiNT is higher than all the other catalysts tested, reaching a maximum of 28 μA cm^{-2} at 350 nm. The result obtained with P25 are similar to the ones obtained by Sharma [24]. The photocurrent response seen with hydrothermally prepared NT is four times higher than the one with P25, which is in agreement with the results obtained with the steady-state potentials (figure S4 (B)).

All photocatalysts show a negative onset potential, -0.16 V for P25, -0.11 V for NT, and -0.3 V for TiNT. The NT electrode has a greater photocurrent at more positive potentials than 0.15 V (SCE) when compared to the P25 electrode. The photocurrent observed was higher than any other photocatalyst tested, with 70 μA cm^{-2} at a potential of +0.5 V (SCE).

The current vs potential response of TiNT can be seen in figure S5. A photocurrent of 75 μA cm^{-2} was observed at a potential of +1.0 V vs SCE. This result is in agreement with the one observed through the measurement at fixed potentials. The photocurrent density for the TiNT electrodes obtained in the present work is slightly higher than that obtained by Sharma [24] who reported 40 μA cm^{-1} at +0.65 V vs SCE with the same reaction conditions, albeit using 0.1 M HClO$_4$. The use of an acidic solution could explain the decrease in photocurrent density as the limiting oxidation reaction occurs more favourably in neutral pH solutions than acidic ones.
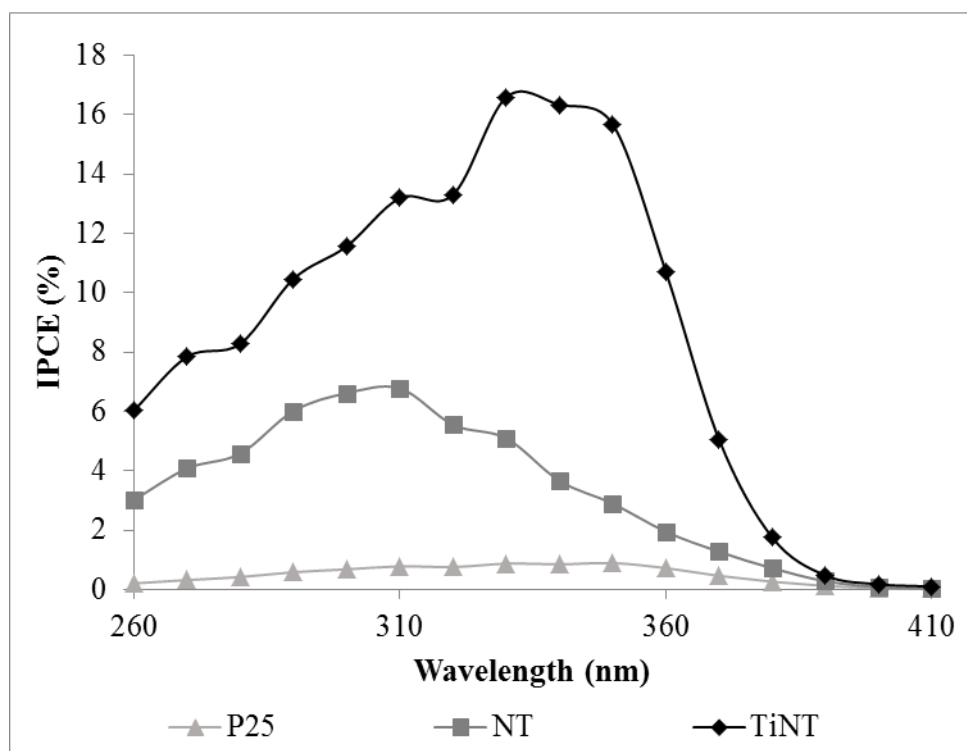
Figure 4 - Combined IPCE plots of P25, hydrothermally prepared NT and TiNT samples

The spectral response of P25, hydrothermally prepared NT and TiNT was used to calculate the IPCE (eq. 2). The IPCE plots for all samples can be seen in figure 4. TiNT show a higher IPCE than the other two photocatalysts. Wang et al. [28], studied the photoelectrochemical properties of P25 and hydrothermally obtained NT. They obtained a peak λ IPCE of 49.3 % for P25 and 17.9 % for NT, while irradiating with a 150 W xenon lamp [28]. The high efficiency obtained by Wang et al, when compared to the ones in this work, can be explained by the difference in light intensities. Light intensity directly affects the IPCE, causing a difference in magnitude and even the shape of the curve measured [29]. A higher IPCE will be obtained at lower light intensities since less recombination will occur and the reaction is not mass transport limited.

Cui et al. [30], studied TiO_2 nanotube arrays, obtained through electrochemical anodization, for the photoelectrochemical water-splitting. In their work, they used a 150 W Xe lamp, Pt wire as counter-electrode, and Ag/AgCl (KCl saturated) as reference electrode. Cui et al. observed an IPCE of around 20 % in the wavelength range from 300 to 370 nm at 0.23 V vs Ag/AgCl for TiNT [30]. Wherein the shape of the IPCE curve is in agreement with the one obtained in this work, but the IPCE value is fairly similar.

TiNT electrodes presented a higher photocurrent density and a more negative onset potential for anodic current when compared to the other electrode materials tested. Therefore, it was selected for the photoanode material in the PEC.

3.3. Photoelectrocatalytic reduction of CO_2

The anode (TiNT) and the cathode, either as received carbon cloth or platinised carbon cloth (Pt deposition $T_2=10s$) were separated by a Nafion membrane and hot pressed together, creating a photoelectrocatalytic disk, prior to being inserted in the PEC. The distance between the photoanode and the irradiation source was kept the same as that used in the photocatalytic experiments [3] in order to allow comparison of the results. Two different photocatalytic disks were tested: one with non-platinised carbon cloth (TiNT/CC) and one with platinised carbon cloth (denoted TiNT/Pt-CC). For each photocatalytic disk, runs in the dark, in the absence of CO_2 and in the presence of 20% CO_2 were performed in replicate (denoted R1 and R2). In between runs, the reactor was purged for 10 minutes, with the irradiation and applied bias off, before being closed to replicate the experiment.
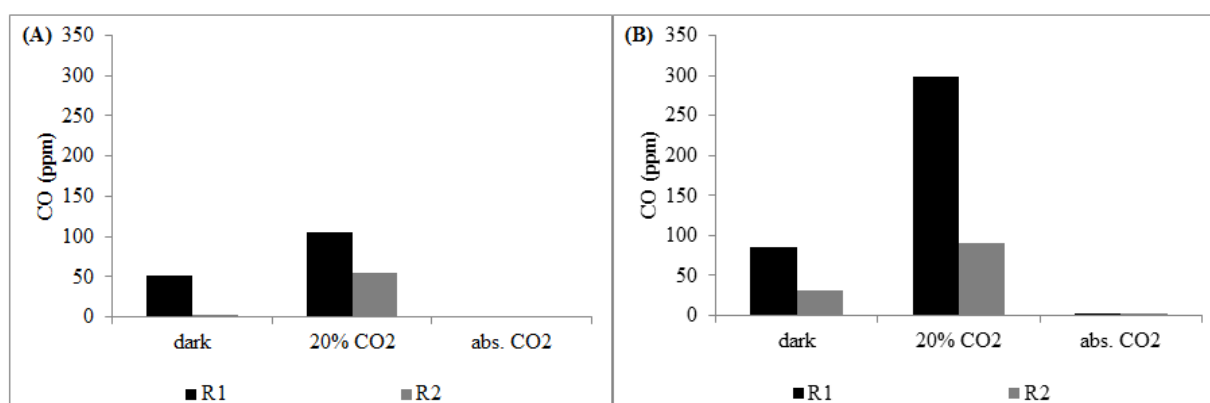

Figure 5 - CO production after 30 min, for both replicates, with both photocatalytic disks tested. (A) TiNT/CC, (B) TiNT/Pt-CC

The results obtained for the photoelectrochemical reduction of CO_2 can be seen in figure 5, where only CO production was observed. In the presence of CO_2 and irradiation, an increase in CO production of 35 % with TiNT/Pt-CC was observed when compared to the TiNT/CC disk (297.98 and 106.04 ppm respectively for R1). The purely electrocatalytic reaction, due to electrical bias, in the dark also showed production of CO, albeit a fraction of the products one seen with light irradiation (84.96 ppm with TiNT/Pt-CC and 51.13 ppm with TiNT/CC for R1).

Controls in the absence of CO_2 were also performed and no product formation was observed for the TiNT/CC disk. However, with the TiNT/Pt-CC disk, a small amount of CO was measured 2.58 ppm for R1 and 2.56 ppm for R2.

A significant difference was observed between R1 and R2 for all reactions, except in the absence of CO_2. The first run always showed a higher production of CO when compared to subsequent runs. With the TiNT/CC disk in the presence of CO_2 and irradiation, the yields of CO decreased from 106.04 ppm to 51.13 ppm whereas with the TiNT/Pt-CC disk, under the same conditions, the yields of CO dropped from 297.98 ppm to 91.17 ppm. This is likely due to poisoning of the cathode. Jovanov et al. reported the lifetime of electrocatalyst for CO_2 reduction is typically short with a half-life in the region of a few hours [31]. The nature of the poisoning was not investigated in this study but candidates include K+ ions coming from the electrolyte, CO or carbonate occupying binding sites for CO_2 reduction on Pt [9, 32]. It has been shown that CO poisons Pt at concentrations of only 10 ppm and can cover from 60 to 100% of the surface of the electrode [33-35]. Considering that on the first run (R1) the lowest amount of CO observed was 84.96 ppm with TiNT/Pt-CC in the dark, and only 10 ppm of CO are enough to poison Pt, we assume that the Pt was poisoned by the production of CO.

Table 1 - Formal Quantum Efficiency (FQE) and Faradaic Efficiency (FE) for CO production obtained for the samples studied

Photocatalytic disk - condition	FQE (250 - 410 nm)		FE (%)	
	R1	R2	R1	R2
TiNT/CC - dark	-	-	20	1
TiNT/CC - light	4.84×10^{-3}	2.93×10^{-3}	4	2
TiNT/Pt-CC - dark	-	-	41	25
TiNT/Pt-CC - light	1.36×10^{-2}	4.16×10^{-3}	13	5

The Formal Quantum Efficiency (FQE) and the Faradaic Efficiency (FE) were calculated based on eq. 3 and 4 respectively for the yields obtained in the photoelectrochemical reduction of CO_2 (table 1). When comparing the FQE obtained in this work with literature [3], even the lowest rate cathode material, TiNT-CC R2, is higher than the ones obtained previously. Using a similar reactor, hydrothermally prepared NT had previously been the best photocatalyst

tested, having a FQE of 2.01×10^{-5} for CO and 5.75×10^{-4} for CH_4 [3]. In this work, the FQE of the photoelectrochemical PEC are two to three orders of magnitude higher than the ones obtained with the photocatalytic reactor. Another important difference between the results obtained in this work and in our previous work [3] is that only CO was observed with PEC whereas CO and CH_4 was obtained with the photocatalytic reactor.

CO has a higher economic value when compared to CH_4. If the PEC was to be commercialised, then high valued low electron number platform chemicals such as CO, COOH, etc would be more desirable since the values per kg are in several orders of magnitude higher than CH_4, CH_3OH, and other fuels. Furthermore, CO is an important ingredient in the feed stock of syngas, with CO_2 and H_2, which through Fischer-Tropsch reactions yields a high number of hydrocarbons [36, 37].

The runs performed in the dark show a high FE for CO, which might suggest that the electrochemical reduction of CO_2 has a higher affinity for CO production. This can be corroborated by the results presented in the literature that show CO as their main product. Sharma et al., studied N-doped CNT for the electrochemical reduction of CO_2. To that end, they used different precursors, such as acetonitrile (ACN), dimethlyformamide (DMF), and triethylamine (TEA), and various growth temperatures; and compared it to pristine CNTs. At a potential of -2.0 V vs SCE, a FE of less than 10 % was obtained for CO with CNTs [38]. Genovese et al., also tested the electrocatalytic reduction of CO_2 in a two-compartment cell with three-electrode, using Pt as a counter electrode. After 1 h of applying a voltage of -1.4 V, 89.8 % of H_2, 0.49 % of hydrocarbons, and 9.8 % of CO was obtained [39]. These results are similar to the ones obtained in this work in the dark, i.e., electrocatalytic reduction of CO_2 to obtain CO.

It is difficult to compare the results obtained in this work to the ones presented in the literature, as most studies reported use a liquid phase reactor. Very few studies have been performed in the gas phase [40-45]. Cheng et al., used a two compartment PEC cell in liquid phase. The photoanode used was Pt-TiNT with 1 M NaCl as the electrolyte and the cathode was Pt-RGO with 1 M $NaHCO_3$ as electrolyte. After 8 h of irradiation with 300 W Xe-arc lamp, the highest product obtained was H_2. Other products, such as alcohols and traces of CO were also observed [44]. Chang et al., used a two-compartment cell, with TiO_2 nanorods (TiO_2 NR) in 0.1 M NaOH as the photoanode, and Pt foil in 0.1 M $KHCO_3$ as cathode. After 3 h, irradiating with a AM 1.5G illumination, FE of 15.86 % for CH_4, 17.05 % for CO, 0.11 % for CH_3OH, and 65.07 %

of H_2 were obtained [42]. Jang et al., used a three-electrode configuration, with Ag/AgCl as reference electrode, Pt mesh as counter electrode, and ZnTe/ZnO–NW as semiconductor in 0.5 M $KHCO_3$. After 30 min of irradiating with a solar simulator (1 sun), they obtained a FE of 7.2 % for CO at -1.2 V vs SCE [41]. Yamamoto et al., used a three electrode PEC, irradiated with a UV LED (365 nm), with TiNT as photoanode in 0.3 M KOH in CH_3OH, Ag quasi-reference electrode (QRE) as reference electrode and Pb or Ag as counter electrode, in 3.0 M $KHCO_3$. With Pb as cathode, a FE of 80 % for $HCOOCH_3$, 9.5 % for CO, and 5.1 % for H_2 was obtained. Whereas a FE of 13 % for $HCOOCH_3$, 61 % for CO, and 3.3 % of H_2 was achieved with Ag as cathode [43]. Showing that electrode material can be utilised to change the main product (Pg cathode for formic acid to CO with Ag cathode) Despite the configuration in the present work being different the FE's for CO are quite similar to the ones observed in the literature.

The photoelectrochemical reduction of CO_2 should have higher photocatalytic efficiency due to the separation of photogenerated electron-hole pairs being increased by an external bias. Additionally, having a two chamber PEC avoids the re-oxidation of reactive products. Despite p-type semiconductors being the most commonly reported in the literature for CO_2 reduction, metal oxide n-type semiconductors are more stable under irradiation in contact with water, and are typically less expensive [6]. In an n-type PEC reactor, the photoanode is commonly composed of a titania-based photocatalyst that will oxidise water to yield O_2 and H^+ under irradiation. The photogenerated electrons and protons are then transported to the other compartment of the cell through the applied bias and the membrane, respectively. Finally, at the electrocatalytic cathode in the gas phase compartment, the protons and electrons react with the CO_2 and generate products [6, 46]. In this work, similarly to the mechanism described by Yamamoto et al. [43], when the TiNT photoanode is irradiated photogenerated electrons and protons are produced from the oxidation reactions. These are then transported to the cathodic gas chamber through the membrane, with help of the applied bias. The electrons/protons react on the cathode surface with the CO_2 present in the compartment following the equation below.

$$CO_2 \xrightarrow{e^-} \bullet CO_2^- \text{ (eq 5)}$$

$$\bullet CO_2^- \xrightarrow{CO_2 + e^-} CO + CO_3^{2-} \text{ (eq 6)}$$
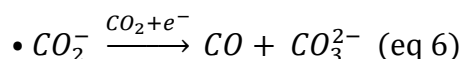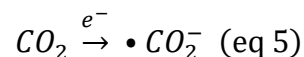
The adsorbed CO_2 (radical anion) in the Pt-CC formed through eq. 5 then follows the second electronation/protonation to produce adsorbed CO (eq. 6). However, as Ampelli et al. stated [9], when using $KHCO_3$ as an anolyte, it also leads to the migration of K^+ through the

membrane. These ions react with the Pt deposited on the CC causing poisoning, which prompts an irreversible deactivation. This could be seen in the present work with the difference in yields between R1 and R2. After R1, some K^+ ions might have been transferred to the cathode, leading to its poisoning and therefore not allowing a reproducible R2.

4. Conclusions

The use of a PEC for the reduction of CO_2 showed a significant improvement in CO product yield when compared to the equivalent photocatalytic reaction (two to three levels of magnitude higher), which is consistent with reports in the literature. Modifying the cathode with Pt also showed a further increase in the CO yields. The FE efficiencies for CO were calculated for all the runs performed in this work. While the ones in the dark are comparable with the ones reported in the literature for electrocatalysis, the same cannot be said for the runs performed with light irradiation as very few reports in the literature use gas phase PECs. However, numerous replicates using PEC are not possible due to poisoning of the cathode [9]. The lifetime of cathode materials for photoelectrocatalytic or photovoltaic reduction of CO2 in PECs is a known issue [31] requiring more robust materials. Further studies utilising alternative membrane and electrode materials could provide an improvement on the limitations of materials observed with this PEC. However this work shows a clear increase in activity when comparing photocatalytic and photoelectrochemical systems under identical irradiation.

6. References
[1] K. Li, X. An, K.H. Park, M. Khraisheh, J. Tang, A critical review of CO2 photoconversion: Catalysts and reactors, Catalysis Today, 224 (2014) 3-12.

[2] F.R. Pomilla, M.A.L.R.M. Cortes, J.W.J. Hamilton, R. Molinari, G. Barbieri, G. Marcì, L. Palmisano, P.K. Sharma, A. Brown, J.A. Byrne, An Investigation into the Stability of Graphitic C3N4 as a Photocatalyst for CO2 Reduction, The Journal of Physical Chemistry C, 122 (2018) 28727-28738.

[3] M.A.L.R.M. Cortes, J.W.J. Hamilton, P.K. Sharma, A. Brown, M. Nolan, K.A. Gray, J.A. Byrne, Formal quantum efficiencies for the photocatalytic reduction of CO2 in a gas phase batch reactor, Catalysis Today, 326 (2018) 75-81.

[4] O. Ola, M.M. Maroto-Valer, Review of material design and reactor engineering on TiO_2 photocatalysis for CO_2 reduction, Journal of Photochemistry and Photobiology C: Photochemistry Reviews, 24 (2015) 16-42.

[5] P. Usubharatana, D. McMartin, A. Veawab, P. Tontiwachwuthikul, Photocatalytic Process for CO2 Emission Reduction from Industrial Flue Gas Streams, Industrial & Engineering Chemistry Research, 45 (2006) 2558-2568.

[6] S. Xie, Q. Zhang, G. Liu, Y. Wang, Photocatalytic and photoelectrocatalytic reduction of CO 2 using heterogeneous catalysts with controlled nanostructures, Chemical Communications, 52 (2016) 35-59.

[7] L.J. Minggu, W.R. Wan Daud, M.B. Kassim, An overview of photocells and photoreactors for photoelectrochemical water splitting, International Journal of Hydrogen Energy, 35 (2010) 5233-5244.

[8] S. Das, W.M.A. Wan Daud, Photocatalytic CO2 transformation into fuel: A review on advances in photocatalyst and photoreactor, Renewable and Sustainable Energy Reviews, 39 (2014) 765-805.

[9] C. Ampelli, G. Centi, R. Passalacqua, S. Perathoner, Synthesis of solar fuels by a novel photoelectrocatalytic approach, Energy & Environmental Science, 3 (2010) 292-301.

[10] S. Das, W.M.A. Wan Daud, A review on advances in photocatalysts towards CO2 conversion, RSC Advances, 4 (2014) 20856-20893.

[11] S. Das, W.M.A. Wan Daud, RETRACTED: Photocatalytic CO2 transformation into fuel: A review on advances in photocatalyst and photoreactor, Renewable and Sustainable Energy Reviews, 39 (2014) 765-805.

[12] Y. Yang, S. Ajmal, X. Zheng, L. Zhang, Efficient nanomaterials for harvesting clean fuels from electrochemical and photoelectrochemical CO 2 reduction, Sustainable Energy & Fuels, 2 (2018) 510-537.

[13] C. Ampelli, R. Passalacqua, S. Perathoner, G. Centi, Nano-engineered materials for H2 production by water photo-electrolysis, Chem. Eng. Trans, 17 (2009) e1016.

[14] E. Kalamaras, M.M. Maroto-Valer, M. Shao, J. Xuan, H. Wang, Solar carbon fuel via photoelectrochemistry, Catalysis Today, 317 (2018) 56-75.

[15] M. Halmann, Photoelectrochemical reduction of aqueous carbon dioxide on p-type gallium phosphide in liquid junction solar cells, Nature, 275 (1978) 115.

[16] C. Ampelli, R. Passalacqua, C. Genovese, S. Perathoner, G. Centi, A novel photo-electrochemical approach for the chemical recycling of carbon dioxide to fuels, CHEMICAL ENGINEERING, 25 (2011).

[17] E.E. Barton, D.M. Rampulla, A.B. Bocarsly, Selective Solar-Driven Reduction of CO2 to Methanol Using a Catalyzed p-GaP Based Photoelectrochemical Cell, Journal of the American Chemical Society, 130 (2008) 6342-6344.

[18] B. Aurian-Blajeni, M. Halmann, J. Manassen, Electrochemical measurement on the photoelectrochemical reduction of aqueous carbon dioxide on p-Gallium phosphide and p-Gallium arsenide semiconductor electrodes, Solar Energy Materials, 8 (1983) 425-440.

[19] K.W. Frese, D. Canfield, Reduction of CO 2 on n-GaAs electrodes and selective methanol synthesis, Journal of The Electrochemical Society, 131 (1984) 2518-2522.

[20] M. Le, M. Ren, Z. Zhang, P.T. Sprunger, R.L. Kurtz, J.C. Flake, Electrochemical reduction of CO2 to CH3OH at copper oxide surfaces, Journal of the Electrochemical Society, 158 (2011) E45-E49.

[21] B.R. Eggins, P.K.J. Robertson, E.P. Murphy, E. Woods, J.T.S. Irvine, Factors affecting the photoelectrochemical fixation of carbon dioxide with semiconductor colloids, Journal of Photochemistry and Photobiology A: Chemistry, 118 (1998) 31-40.

[22] D.H. Won, J. Chung, S.H. Park, E.-H. Kim, S.I. Woo, Photoelectrochemical production of useful fuels from carbon dioxide on a polypyrrole-coated p-ZnTe photocathode under visible light irradiation, Journal of Materials Chemistry A, 3 (2015) 1089-1095.

[23] Y. Shin, S. Lee, Self-Organized Regular Arrays of Anodic TiO2 Nanotubes, Nano Letters, 8 (2008) 3171-3173.

[24] P.K. Sharma, M.A.L.R.M. Cortes, J.W.J. Hamilton, Y. Han, J.A. Byrne, M. Nolan, Surface modification of TiO2 with copper clusters for band gap narrowing, Catalysis Today, 321-322 (2017) 9-17.

[25] M.M.E. Duarte, A.S. Pilla, J.M. Sieben, C.E. Mayer, Platinum particles electrodeposition on carbon substrates, Electrochemistry Communications, 8 (2006) 159-164.

[26] J.A. Byrne, A. Davidson, P.S.M. Dunlop, B.R. Eggins, Water treatment using nano-crystalline TiO2 electrodes, Journal of Photochemistry and Photobiology A: Chemistry, 148 (2002) 365-374.

[27] K.C. Schwartzenberg, K.A. Gray, Nanostructured Titania: the current and future promise of Titania nanotubes, Catalysis Science & Technology, 2 (2012) 1617-1624.

[28] D. Wang, B. Yu, F. Zhou, C. Wang, W. Liu, Synthesis and characterization of anatase TiO2 nanotubes and their use in dye-sensitized solar cells, Materials Chemistry and Physics, 113 (2009) 602-606.

[29] G. Palma, L. Cozzarini, E. Capria, A. Fraleoni-Morgera, A home-made system for IPCE measurement of standard and dye-sensitized solar cells, Review of Scientific Instruments, 86 (2015) 013112.

[30] H. Cui, W. Zhao, C. Yang, H. Yin, T. Lin, Y. Shan, Y. Xie, H. Gu, F. Huang, Black TiO2 nanotube arrays for high-efficiency photoelectrochemical water-splitting, Journal of Materials Chemistry A, 2 (2014) 8612-8616.

[31] Z.P. Jovanov, J. Ferreira de Araujo, S. Li, P. Strasser, Catalyst Preoxidation and EDTA Electrolyte Additive Remedy Activity and Selectivity Declines During Electrochemical CO2 Reduction, The Journal of Physical Chemistry C, 123 (2019) 2165-2174.

[32] K. Jambunathan, B.C. Shah, J.L. Hudson, A.C. Hillier, Scanning electrochemical microscopy of hydrogen electro-oxidation. Rate constant measurements and carbon monoxide poisoning on platinum, Journal of Electroanalytical Chemistry, 500 (2001) 279-289.

[33] J.G. Love, A.J. McQuillan, Potential dependent FTIR spectra of carbon monoxide adsorbed at the platinum electrode/absolute methanol solution interface, Journal of Electroanalytical Chemistry and Interfacial Electrochemistry, 274 (1989) 263-270.

[34] B. Beden, F. Hahn, J.-M. Leger, C. Lamy, M.I.d.S. Lopes, "In situ" infrared reflectance spectroscopic study of the adsorbed species resulting from CH3OH adsorption on polycrystalline Pt in acid solution, Journal of Electroanalytical Chemistry and Interfacial Electrochemistry, 258 (1989) 463-467.

[35] H. Igarashi, H. Uchida, M. Suzuki, Y. Sasaki, M. Watanabe, Removal of carbon monoxide from hydrogen-rich fuels by selective oxidation over platinum catalyst supported on zeolite, Applied Catalysis A: General, 159 (1997) 159-169.

[36] M.R. Shaner, H.A. Atwater, N.S. Lewis, E.W. McFarland, A comparative technoeconomic analysis of renewable hydrogen production using solar energy, Energy & Environmental Science, 9 (2016) 2354-2371.

[37] Q. Lu, F. Jiao, Electrochemical CO2 reduction: Electrocatalyst, reaction mechanism, and process engineering, Nano Energy, 29 (2016) 439-456.

[38] P.P. Sharma, J. Wu, R.M. Yadav, M. Liu, C.J. Wright, C.S. Tiwary, B.I. Yakobson, J. Lou, P.M. Ajayan, X.D. Zhou, Nitrogen-doped carbon nanotube arrays for high-efficiency electrochemical reduction of CO2: on the understanding of defects, defect density, and selectivity, Angewandte Chemie International Edition, 54 (2015) 13701-13705.

[39] C. Genovese, C. Ampelli, S. Perathoner, G. Centi, Electrocatalytic conversion of CO2 on carbon nanotube-based electrodes for producing solar fuels, Journal of Catalysis, 308 (2013) 237-249.

[40] H. Pang, G. Yang, P. Li, H. Huang, F. Ichihara, T. Takei, J. Ye, Wafer-scale Si nanoconed arrays induced syngas in the photoelectrochemical CO2 reduction, Catalysis Today, (2019).

[41] Y.J. Jang, J.-W. Jang, J. Lee, J.H. Kim, H. Kumagai, J. Lee, T. Minegishi, J. Kubota, K. Domen, J.S. Lee, Selective CO production by Au coupled ZnTe/ZnO in the photoelectrochemical CO2 reduction system, Energy & Environmental Science, 8 (2015) 3597-3604.

[42] X. Chang, T. Wang, P. Zhang, Y. Wei, J. Zhao, J. Gong, Stable aqueous photoelectrochemical CO2 reduction by a Cu2O dark cathode with improved selectivity for carbonaceous products, Angewandte Chemie International Edition, 55 (2016) 8840-8845.

[43] T. Yamamoto, H. Katsumata, T. Suzuki, S. Kaneco, Photoelectrochemical Reduction of CO2 in Methanol with TiO2 Photoanode and Metal Cathode, ECS Transactions, 75 (2017) 31-37.

[44] J. Cheng, M. Zhang, G. Wu, X. Wang, J. Zhou, K. Cen, Photoelectrocatalytic Reduction of CO2 into Chemicals Using Pt-Modified Reduced Graphene Oxide Combined with Pt-Modified TiO2 Nanotubes, Environmental Science & Technology, 48 (2014) 7076-7084.

[45] Q. Wang, X. Wang, Z. Yu, X. Jiang, J. Chen, L. Tao, M. Wang, Y. Shen, Artificial photosynthesis of ethanol using type-II g-C3N4/ZnTe heterojunction in photoelectrochemical CO2 reduction system, Nano Energy, 60 (2019) 827-835.

[46] G. Centi, S. Perathoner, Heterogeneous Catalytic Reactions with CO2: Status and Perspectives, in: S.-E. Park, J.-S. Chang, K.-W. Lee (Eds.) Studies in Surface Science and Catalysis, Elsevier2004, pp. 1-8.